DYNAMICAL STUDY OF A MOORED VESSEL USING COMPUTER VISION

Andres Figuero
Water and Environmental Engineering Group (GEAMA), Universidade da Coruña, Campus Elviña s/n 15071, A Coruña, Spain, andres.figuero@udc.es

Alvaro Rodriguez
Department of Physics, Umeå University, Linneaus Väg, SE-901 87 Umeå, Sweden.

Jose Sande
Water and Environmental Engineering Group (GEAMA), Universidade da Coruña, Campus Elviña s/n 15071, A Coruña, Spain

Enrique Peña
Water and Environmental Engineering Group (GEAMA), Universidade da Coruña, Campus Elviña s/n 15071, A Coruña, Spai

Juan R Rabuñal
Department of Computer Science, and Centre of Technological Innovations in Civil Engineering, University of A Coruña, Campus Elviña s/n 15071, A Coruña, Spain

DYNAMICAL STUDY OF A MOORED VESSEL USING COMPUTER VISION

DYNAMICAL STUDY OF A MOORED VESSEL USING COMPUTER VISION

Andres Figuero[1], Alvaro Rodriguez[2], Jose Sande[1], Enrique Peña[1], and Juan R. Rabuñal[3]

ABSTRACT

Wind and wave effects have a major impact on the design of mooring and anchoring systems, whose purpose is to prevent the movement of the cargo and the moored ship while optimizing the operations which have to take place in port.

The dynamic behavior of a ship moored in waves has been mathematically described and interactions between ships and environmental loads have been commonly tested for different docks and mooring systems in scale models. However, the behavior of real ships in true mooring conditions has not been properly addressed in scientific literature.

This paper proposes a novel computer vision technique to monitor moored ships. This approach uses the correlation of visual features in the images of the ship to estimate its movements along time.

The proposed technique has been validated in laboratory conditions and applied in a real scenario to study the behavior of the ship Urania Mella in the Outer Port of A Coruña (Spain), in Punta Langosteira, obtaining very promising results.

I. INTRODUCTION

Seaports are areas for berthing or anchoring ships where there is the equipment for the transfer of goods between ship and shore or between ships. Currently they should be considered not only one of the most important aspects of maritime transport but also one of the most vital aspects of a national transport infrastructure (Alderton, 2008).

There are various means of holding a ship to a dock or pier. The most common nowadays consists in tying the ship to the

Fig. 1. The ship Urania Mella, analyzed in the tests conducted in this paper, moored in the dock of A Coruña.

harbor with lines made of natural or artificial materials relying on the experience of the operator. In general, the lower the magnitude of the loads to be absorbed by the mooring system, the more freely the ship is left to move. However, reducing the amplitude of motions in moored ships is also crucial to increase the efficiency of loading operations, to minimize port operational costs, as well as to reduce security and environmental risks (Malheiros et al., 2013). Fig. 1 shows a ship using this mooring system.

The need to optimize dock operations while minimizing the risk of damages in the ship, dock and cargo challenged several researchers to describe mathematically the behavior of a ship moored in waves. The first milestone in these researches was achieved in the 50 s, in works such as Finkelstein (1957) where a time-domain method was applied to describe waves not as the sum of regular wave components, but as a summation of impulsive sources. Later works (Wehausen, 1967) used this approach to formulate a solution for a floating body making an impulsive displacement and to calculate the wave forces for a fixed body in waves.

The modeling of ship motion was first proposed by Cummins (1962). According to this model, a moored ship is considered as a body floating in an incompressible, homogeneous and irrotational fluid. An arbitrary motion of the ship can be mathematically described as follows (Cummins, 1962):

$$(M + A)\vec{\ddot{X}}(t) + B\vec{\dot{X}}(t) + C\vec{X}(t) + \int_0^\infty K(\tau)\vec{\dot{X}}(t-\tau)d\tau = \vec{F}(t) \quad (1)$$

Where M is the inertia matrix. A, B and C are the matrices

for the added mass, linearized viscous damping and hydrostatic restoring respectively. *K* contains the impulse response functions. *X* is the position of the floating body. *F* represents the applied forces (forcing function). The added mass coefficients and impulse response functions can be determined directly with a time-domain boundary-integral model following Cummins (1962) and Beck and Liapis (1987).

In a more practical approach, the motion of a mooring ship can be studied according to its degrees of freedom. Therefore, the ship movement can be categorized in basic movements. Some of these movements are strongly dependent on the features of the hull and the load condition, and are not significantly altered by mooring. These are the natural oscillation modes of the ship: the rotation about the longitudinal axis (roll), related to transverse stability; the rotation about the transverse axis (pitch), related to longitudinal stability; and the vertical translation motion (heave), depending on the floating area.

The moored ship presents three additional oscillation modes: longitudinal motion (surge); lateral motion (sway); and the rotation about the vertical axis (yaw). These motions have periods higher than the previous ones, and are strongly influenced by the characteristics of the mooring and anchoring system (Pina and Alonso, 1993).

However, while these mechanics are well known, the driving mechanisms in harbor hydrodynamics are complex. Therefore, in addition to currents, wind forces and tides, the interaction of these elements with each other and with harbor infrastructures may have major influence in the seaport functioning. Furthermore, the risk of damaging moored ships or breaking mooring lines can be dramatically increased due to complex phenomena such as harbor oscillations. They are caused by small amplitude and large wavelength waves entering from the sea. These may induce large horizontal moored ship motions because their frequency is close to the natural frequency of the system made of the ship, the mooring lines and the fenders (Rabinovich, 2009; Uzaki et al., 2010).

To deal with these problems, a wide range of hydrodynamic studies has been carried out in order to characterize conditions in different ports (González-Marco et al., 2008; Grifoll et al., 2009; Sammartino et al., 2014). However, one of the established techniques to measure the movements of moored ships in actual operation conditions is based on the use of Differential GPS (DGPS) positioning systems on board (Bont et al., 2010; Ge et al., 2011). This technique implies the use of expensive devices on the moored ships making these systems unpractical in most scenarios.

In this work, a technique based on the analysis of images of moored ships is proposed. This technique uses a set of video cameras to record the ship while is moored in a harbor, and measures the movement through the tracking of feature points.

Computer vision techniques have been widely applied in naval and maritime applications. Broggi et al. (2012) described a speed warning system for boats moving in a navigation channel, Yun Jip et al. (2014) presented an automatic ship detection method in harbor areas and Malheiros et al. (2013) applied a stereoscopic vision system to measure the motion of rigid bodies in laboratory tests. These applications are commonly based on the use of a Kalman filter to track a navigating ship. Other examples include the use of local self-similarity to detect ships in harbor areas (Hu et al., 2009) or the use of a dynamic ship model into a factor graph for ship tracking (Castaldo and Palmieri, 2014).

However, only few examples exist in literature where the movement of moored ships has been studied such as Malheiros et al. (2009) who used stereo cameras to track sets of marks placed on a model of a moored oil tanker by means of determining the best fit plane using least squares. This work was later refined in Malheiros et al. (2013) to include a Kalman filter. Important drawbacks in this research were that assays had only been conducted in indoor and controlled light conditions, without addressing the issues of a real scenario, where weather and light changes may represent important challenges. Furthermore, the use of special sets of marks in a high-contrast background of not negligible size is impractical for its use in a real ship.

The aforementioned works show the potential of computer vision to monitor the oscillations of a moored ship, and this paper presents a novel technique to deal with this question, based on the analysis of sequences of images of the vessel in field conditions.

II. PROPOSED TECHNIQUE

With the purpose of estimate the motion of the ship, firstly a set of cameras is calibrated and installed through the seaport facilities, with different points of view of the moored ship. Secondly, a set of features is selected for each view and tracked along the corresponding image sequence. Finally, the displacement information is then integrated to extract the 3D motions of the ship.

1. Calibration

To be able to obtain real scale measurements, cameras must be synchronized and calibrated. To this end, 2D and 3D camera systems can be used. While the functioning of the proposed technique is similar in both scenarios, there are important differences in the calibration process that may be pointed out.

In the 2D camera system, each camera tracks different features and is calibrated separately using the pin-hole camera equations (Zhang, 1999) expressed as follows:

$$
\begin{bmatrix} x_i \\ y_i \\ 1 \end{bmatrix} = M_{3x3} \times \begin{bmatrix} X_c/Z_c \\ Y_c/Z_c \\ 1 \end{bmatrix} \quad M = \begin{bmatrix} f_x & 0 & c_x \\ 0 & f_y & c_y \\ 0 & 0 & 1 \end{bmatrix} \quad (2)
$$

where (X_c, Y_c, Z_c) are the coordinates of a point in the camera space, (x_i, y_i) are the corresponding pixel coordinates, *M* is the transformation matrix, $f(f_x, f_y)$ represents the focal length and

$c(c_x, c_y)$ determines the optical center, establishing as reference the image coordinates where a point is projected through the center of the lens. In practice, due to small imperfections in the lens and other factors, some distortions are integrated into the image. These distortions can be modeled using the following parametric equations (Weng et al., 1992):

$$dr_x(x) = xk_1r^2 + xk_2r^4 + xk_3r^6$$
$$dr_y(y) = yk_1r^2 + yk_2r^4 + yk_3r^6$$
$$dt_x(x,y) = k_3(r^2 + 2x^2) + 2k_4xy \quad (3)$$
$$dt_y(x,y) = 2k_3xy + k_4(r^2 + 2y^2)$$

where x and y are spatial coordinates, r is the distance to the lens optical center, dr is the radial distortion, dt is the tangential distortion and k_i are the distortion parameters to be determined.

In this case, the calibration is performed taking into account the real geometry of a 2D pattern of features. The types of motions which can be measured depend on the amount and position of the cameras.

On the other hand, in a 3D camera system, two or more cameras are used to observe the same set of features. Here, the calibration process consists in determining the structure of the scene from the two or more views. This technique consists in the calibration of each one of the cameras using the same process as in a 2D case and then obtaining the estimation of the translation vectors ($T_{1\times3}$) and rotation matrix ($R_{3\times3}$) of the second camera relative to the first one. This can be expressed as follows:

$$\begin{bmatrix} X_c \\ Y_c \\ Z_c \end{bmatrix} = R_{3\times3} \times \begin{bmatrix} X \\ Y \\ Z \end{bmatrix} + T_{1\times3}$$

$$R = \begin{bmatrix} r_{11} & r_{12} & r_{13} \\ r_{21} & r_{22} & r_{23} \\ r_{31} & r_{32} & r_{33} \end{bmatrix} \quad T = \begin{bmatrix} t_1 \\ t_2 \\ t_3 \end{bmatrix} \quad (4)$$

where (X, Y, Z) are the coordinates of the point in the real world, and (X_c, Y_c, Z_c) in the camera coordinate system (or reference coordinate system). The entire process is described in detail in Hannah (1974) and Bolles et al. (1993).

While the use of 3D camera systems has several advantages, they are not suitable for a general scenario, since their working distance is highly dependent of the camera baseline, and available 3D camera systems are not accurate in distances higher than 20 m, which are required for big ships in commercial ports. Therefore, in this paper, a 2D camera system was used in the conducted experiments.

2. Feature Selection

To select the points of interest which will be used to match the image, a semiautomatic approach was conducted consisting in three main steps:

(1) In the first step, the user selects a region of interest in one of the images of the ship, this region should ideally correspond with a part of the ship located in its sagittal or frontal plane, according to the motion of interest.
(2) Later, in the second step, an automatic technique for feature detection is applied. In this work, the Speeded Up Robust Features (SURF) technique (Bay et al., 2008) was used. This is a scale-invariant feature detector based on the Hessian-matrix. The Hessian is calculated using approximate second-order Gaussian derivatives in the form of box-type filters (Tuytelaars and Mikolajczyk, 2008). The scale invariance is warranted by bandpass multi-resolution pyramid decomposition.
(3) Finally, the user has the chance to add, edit or modify the resulting points.

3. Search Process

After selecting the features of interest, the strategy employed to track these features is based on an iterative multi-resolution pyramidal process. This search process is based in comparing the regions around the points of interest in the original image with the ones representing a candidate displacement according to a motion model. Here the Pearson correlation quotient (R) is used as similarity metric. The search process is divided in two stages:

(1) First order motion model:
   In this stage, the search process is restricted to find a rigid transformation of the scene. To this end, three degrees of freedom are used to represent the main effects of motion expressed as follows:

$$X_i' = X_i - C_X\cos(\alpha) + C_Y\sin(\alpha) + C_X + d_X$$
$$Y_i' = Y_i - C_X\sin(\alpha) + C_Y\cos(\alpha) + C_Y + d_Y \quad (5)$$

   where, (X_i, Y_i) and (X_i', Y_i') represent image coordinates before and after the first displacement of the feature i, α is a 2D rotation angle relative to the center of the image (C_X, C_Y) and (d_X, d_Y) represent a linear displacement.
   This first order motion model is used with the pyramidal decomposition in a coarse-to-fine approach. Therefore, the first iteration is executed with a subsampled image and in a wide search area. To this end, a maximum rotation angle and linear displacement is selected by the user. Later, in each iteration the image resolution is increased by a factor of 2, while the search range of motions is reduced accordingly. This technique increases accuracy along time and reduces computational cost. The number of pyramidal steps and the iterations in full resolution can also be set by the user.
(2) Second order motion model:
   After obtaining the global similarity maximum in the pre-

vious step, the motion measurement is refined with a second search process to find locally linear displacements for each feature of interest. This can be represented as follows:

$$x_i^d = X_i' + l_x$$
$$y_i^d = Y_i' + l_Y \tag{6}$$

where (x_i^d, y_i^d) represent the refined coordinates of the feature i, after a discrete linear displacement determined by (l_X, l_Y).

With this technique, for each feature the maximum discrete correlation value lead us to the most probable linear displacement and to obtain a subpixel accuracy, the correlation values must be translated to a continuous space. To this end, the true peak of the similarity is calculated by fitting a Gaussian function in each dimension of the movement using three points to solve each equation. This can be expressed as follows for the x dimension of displacement:

$$x_i^c = x_i^d + \frac{N}{D}$$
$$N = \ln\left(R\left(x_i^d - 1\right)\right) - \ln\left(R\left(x_i^d + 1\right)\right) \tag{7}$$
$$D = 2\ln\left(R\left(x_i^d - 1\right)\right) - 4\ln\left(R\left(x_i^d - 1\right)\right) + 2\ln\left(R\left(x_i^d + 1\right)\right)$$

where x_i^c represent the coordinates of the feature i in a continuous space after a local linear displacement, being the maximum discrete correlation value for the feature in the dimension x noted as $R(x_i^d)$.

After this step, the local displacements of the features are constrained to a parametric global motion model using the Gauss-Newton method to solve an overdetermined homography transformation (8-parameter nonlinear transformation). This can be expressed as follows:

$$X_i'' = \left(x_i^c h_1 + y_i^c h_2 + h_3\right) / \left(x_i^c h_7 + y_i^c h_8 + 1\right)$$
$$Y_i'' = \left(x_i^c h_4 + y_i^c h_5 + h_6\right) / \left(x_i^c h_7 + y_i^c h_8 + 1\right) \tag{8}$$

where (X_i'', Y_i'') represent image coordinates after the second order motion model and h_k are the homography parameters which are calculated from the previous values.

4. Long Term Tracking

Using the previous technique, it is possible to track the initial set of features in time. However, when tracking is performed during several hours, the scene will suffer dramatic lighting and color changes due to the day-night cycle, and to changes in meteorological conditions like clouds, fog or rain. Additionally, it is expected that the image will be out of focus in some frames and that extraneous bodies, such as seagulls or the crew, will interfere with the scene, occluding some of the features of interest.

Therefore, the algorithm must be able to handle occlusions and it must be robust against focus errors and fast intensity changes. Additionally, it must be able to adapt to long term changes in the scene. These issues have been addressed in different ways:

Firstly, occlusions are handled by the first order motion model, allowing the use of a subset of features in the search process. To this end, features with a low correlation are disregarded when the majority of them have achieved a good match. Additionally, in this scenario the second order search process will not update the position of a feature with low correlation. This threshold can be set by the user, its default value being 0.5.

Secondly, the used Pearson similarity metric is invariant to the average of intensity. This provides robustness to fast and short lighting changes. Furthermore, the use of a neighborhood of interest to correlate each of the features, allows achieving a high level of correlation when the image is out of focus as a consequence of large motions of the tracking object that cause its way out of the focus area manually fixed at the beginning of the monitoring.

Finally, to overcome slow and long term changes in the scene, the tracked features are updated along time, refreshing the source image after at a certain time rate selected by the user. To this end, the source point of the measurement is dynamically updated using the previous displacements to follow the position of the original features in the vessel. This strategy has been applied successfully with a block-matching algorithm in works such as Rodriguez et al. (2012) where the procedure is explained in detail.

III. EXPERIMENTAL RESULTS

1. Laboratory Experiments

To validate the technique proposed in this paper, a set of experiments were conducted in the Center of Technological Innovations in Construction and Civil Engineering (CITEEC) of the University of A Coruña.

The conducted experiments were recorded with a video camera and also with an Inertial Measurement Unit (IMU). The IMU is the main component of inertial navigation systems (Phuong et al., 2009; Ayub et al., 2012). It allows to estimate the position and orientation tracking of a moving body relative to a known starting point. Although IMUs usually require to be used in combination with absolute positioning systems to rule out long term errors (Woodman, 2007), they can be used to estimate angular movements without external references. With this purpose, the selected IMU was equipped with three different type of sensors. A 3-axis microelectromechanical (MEMs) gyroscope used to measure the angular velocity of the body (STMicroelectronics L3GD20H). A 3-axis accelerometer to obtain the accelerations of the moving object relative to itself (STMicroelectronics LSM303DLHC). And finally, three orthogonal anisotropic magneto-resistive (AMR) sensors to measure the strength and direction of the local magnetic field (STMicroelectronics LSM303DLHC). The integration of these sensors allows obtaining a robust IMU. The device was previously calibrated in dif-
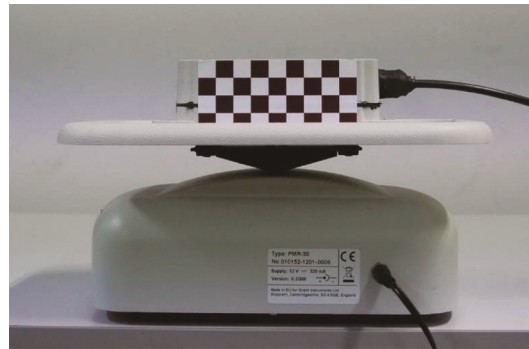
Fig. 2. IMU device placed on top of the rocker with a chess pattern used to record the oscillations with the computer vision system.
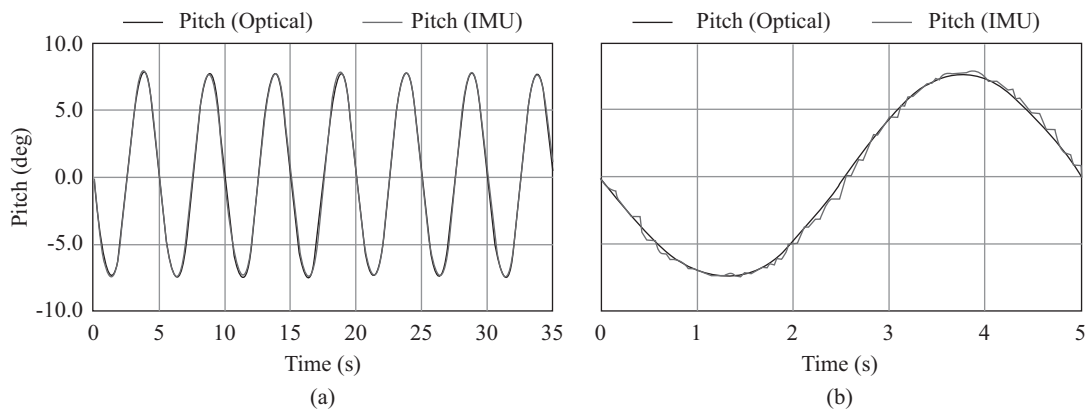

Fig. 3. Rocker movement recorded with the proposed technique and the IMU device for a 15.0º oscillation amplitude and 0.2 Hz frequency (a). One oscillation cycle sample of the same test (b).
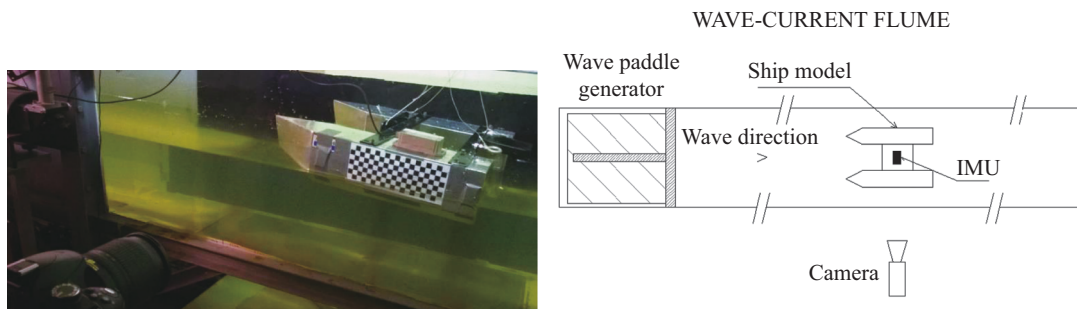

Fig. 4. Experimental assembly used in the comparative assays performed in the Center of Technological Innovations in Construction and Civil Engineering (CITEEC) of the University of A Coruña.

ferent laboratory tests, in order to measure and compare the precision of the system. The obtained results showed a precision up to 0.2°.

In the first tests conducted in the CITEEC, a fixed-angle platform rocker with a periodic oscillating movement of 15.0° constant amplitude was used to compare the accuracy of both the video camera and the IMU techniques. This rocker was programmed to describe a movement of 0.2 Hz oscillation frequency. The IMU was placed with its longitudinal axis perpendicularly aligned to the rotation axis of the rocker (Fig. 2). Oscillations were recorded during a period of 35 s using both techniques.

Fig. 3(a) shows the result of the rocker test. A strong correlation between the measurements of both techniques was observed, with a Pearson correlation coefficient of 0.99. Furthermore, the mean value of the oscillation amplitude was 15.20° and 14.96° for the IMU and the computer vision system, respectively. Taking into account that the oscillation amplitude of the rocker was 15.0°, the proposed technique showed a higher accuracy and uniformity in the movement record than the IMU which was noisier (Fig. 3(b)).

The second tests were conducted in the $25.0 \times 0.8 \times 0.6$ m wave current flume located in the CITEEC. The IMU was aligned with the longitudinal axis of a scale ship model and the

Table 1. Pearson Correlation Coefficient analysis of the Pitch.

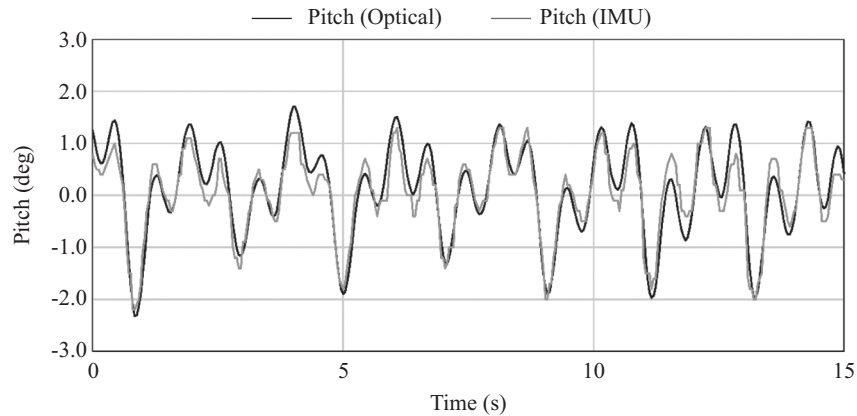| Correlation		Wave Height		
		18 cm	20 cm	24 cm
Wave Frequency	0.5 Hz	0.93	0.81	0.93
	0.7 Hz	0.95	0.93	0.96

Fig. 5. A 15 seconds duration sample of Pitch measurements with the proposed technique and the IMU device for a wave height of 18 cm and a wave frequency of 0.5 Hz.
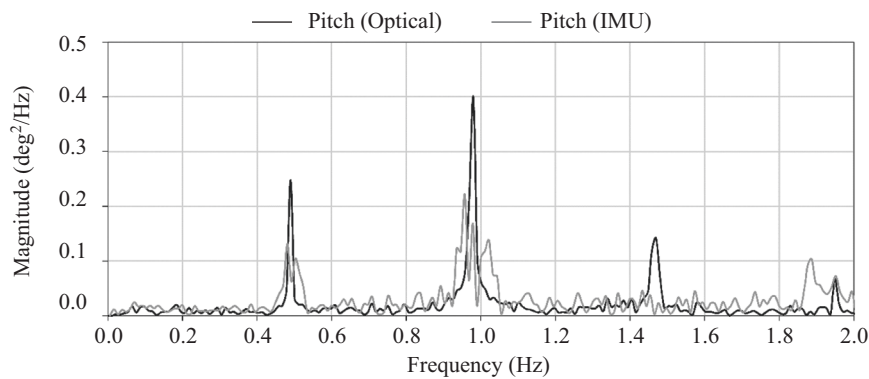

Fig. 6. Frequency spectrum of Pitch measured with the proposed technique and the IMU device for a wave height of 18 cm and a wave frequency of 0.5 Hz.

pitch was measured for different wave height and frequencies.

The experimental setup used in these experiments is shown in Fig. 4.

Examples of obtained results are shown in Figs. 5-8.

Frequency spectra and waveform comparisons in Figs. 5-8 and the Pearson correlation coefficients in Table 1 clearly show how the proposed technique and the IMU device provided almost identical results, although the IMU device presented noisier measurements. This noise was also observed in the rocker test (Fig. 3(b)) even describing a more controlled movement than the generated in the wave flume. This effect is probably induced by the higher accuracy of this device.

2. Field Campaign

To validate the technique proposed in this paper in this pa-per in real field conditions, a set of assays was performed to measure the dynamic behavior of the ship Urania Mella, a 2009 antipollution vessel of 72 m length × 15 m beam and dead-weight tonnage of 3,180 tons.

The Urania Mella was moored in the Outer Port of A Coruña (Spain), in Punta Langosteira. The port structure is composed of a 3.300 m length main breakwater, a 400 m length spur break-water and a 900 m length vertical wall dock with an average water depth of 22 m, where the analyzed vessel was moored (Fig. 9). This port faces the North Atlantic Ocean, and is ty-pically exposed to the high energetic swell generated by the low pressures coming from Greenland. The interaction between swell waves generates long waves, also called infragravity waves, which are released as free waves and can be reflected from the beach (Herbers et al., 1995).
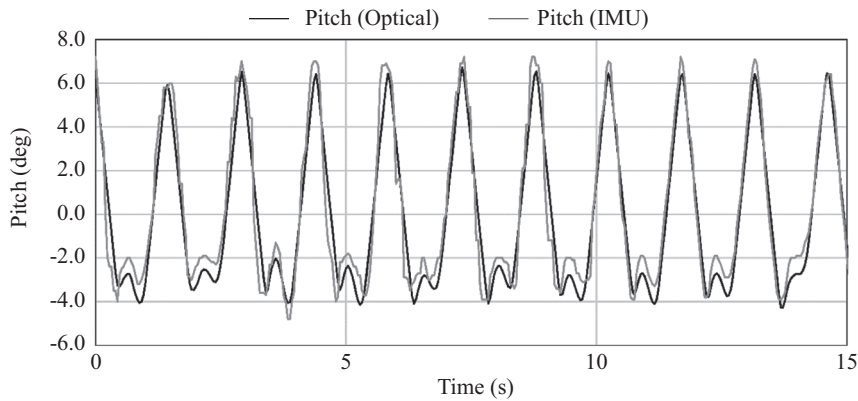
Fig. 7. A 15 seconds duration sample of Pitch measurements with the proposed technique and the IMU device for a wave height of 18 cm and a wave frequency of 0.7 Hz.
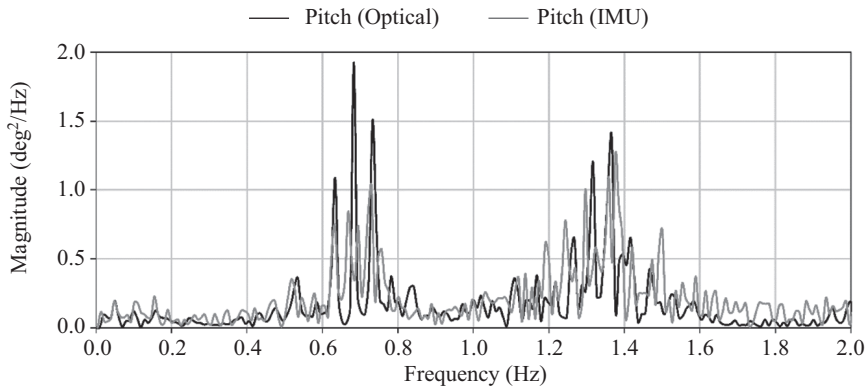

Fig. 8. Frequency spectrum of Pitch measured with the proposed technique and the IMU device for a wave height of 18 cm and a wave frequency of 0.7 Hz.
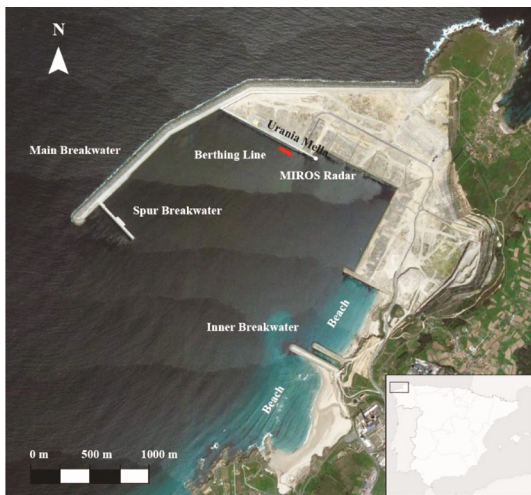

Fig. 9. Outer Port of A Coruña, in Punta Langosteira (Northwest of Spain), and mooring location of the Urania Mella during the assays, and location of the MIROS radar used to measure wave height.
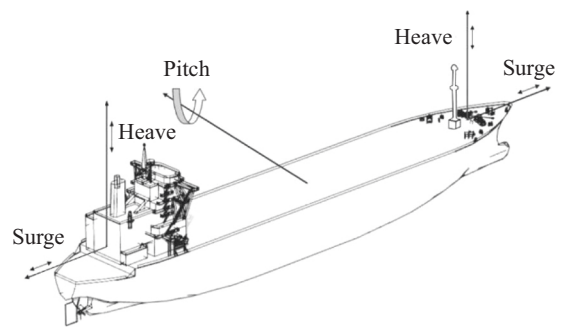

Fig. 10. Oscillation modes of the Urania Mella, measured in the assays.

The periods of the free waves may coincide with the eigen periods of the basin and the natural motion periods of the moored ship, producing harbour resonance and vessel movements amplification.

Finally at the southern part of the port there is a 2.5 km beach where cusp and rhythmic shoreline features have been detected.

The mooring configuration of the vessel was composed of 12 lines distributed in 4 headlines, 2 bow springs, 1 stern spring and 5 sternlines.

In this scenario, surge, heave and pitch were identified as three of the most limiting motions from the point of view of ship operations. This aspect was confirmed during the conversations maintained with different members of the crew.

These motions are illustrated in Fig. 10.

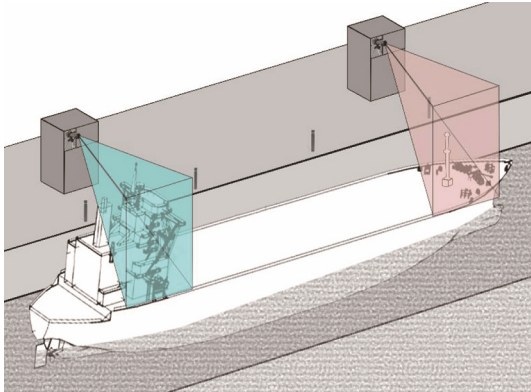To measure these parameters with the proposed technique,

Fig. 11. Image acquisition scheme, the field of view and the location of the cameras used are represented in the image.

Fig. 12. Output of the stern camera during the assays. Selected features and corresponding displacement vectors are marked on the image.
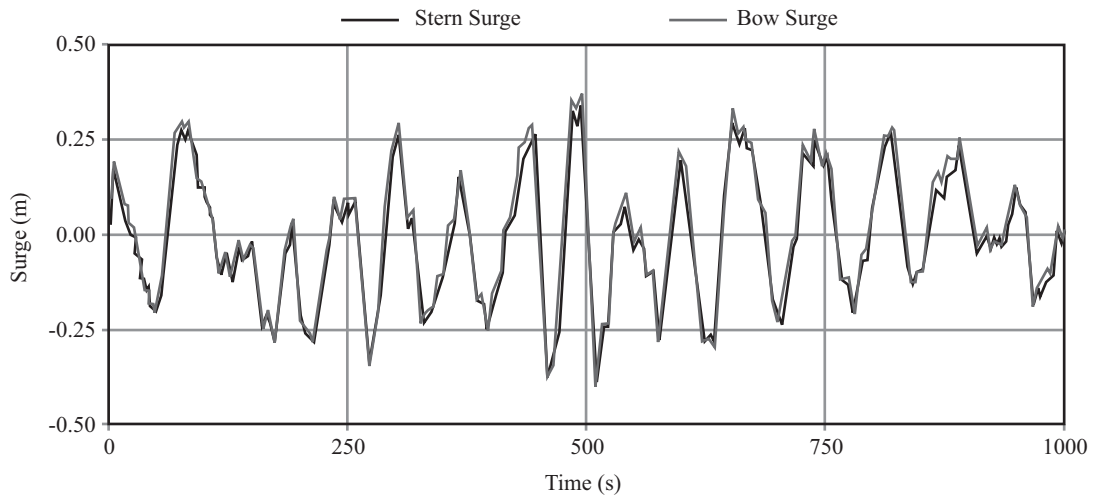

Fig. 13. A 1000 seconds duration sample of Surge measured in the bow and stern of the Urania Mella.
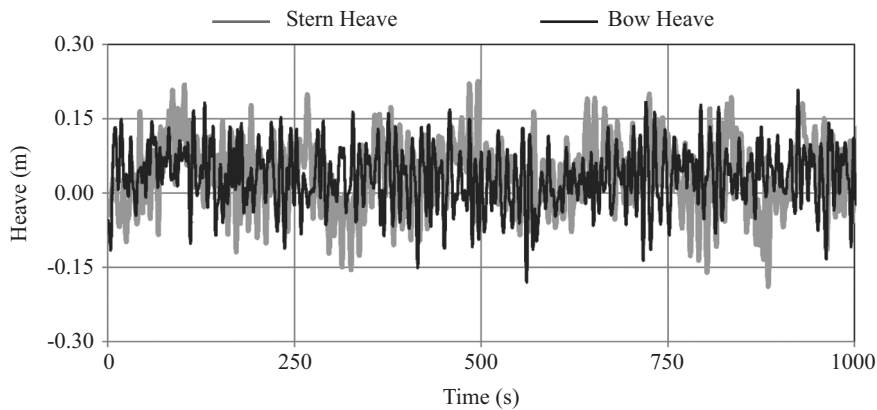

Fig. 14. A 1000 seconds duration sample of Heave measured in the bow and stern of the Urania Mella.

two digital cameras, isolated from atmospheric conditions and equipped with a remote control, were deployed in front of the bow and stern of the Urania Mella (Fig. 11). The positioning of a third camera taking pictures in the direction of the longitudinal axis of the moored vessel would allow recording the other three movements (roll, sway and yaw). Unfortunately the berthing line geometry prevented the placement of this camera and these motions were not analyzed.
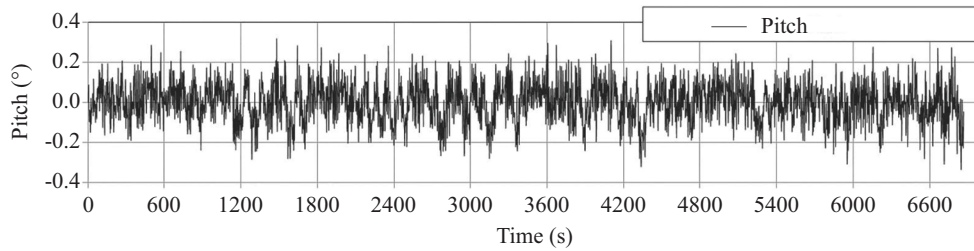
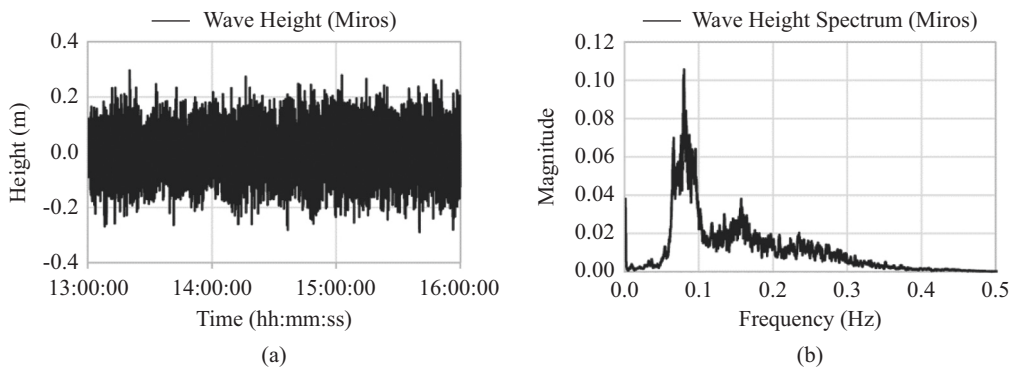**Fig. 15. Pitch calculated from differences in heave, for the Urania Mella.**

(a) (b)

Fig. 16. Evolution of wave height (a), and wave height spectrum (b) measured with MIROS radar, which measures the free surface elevation.
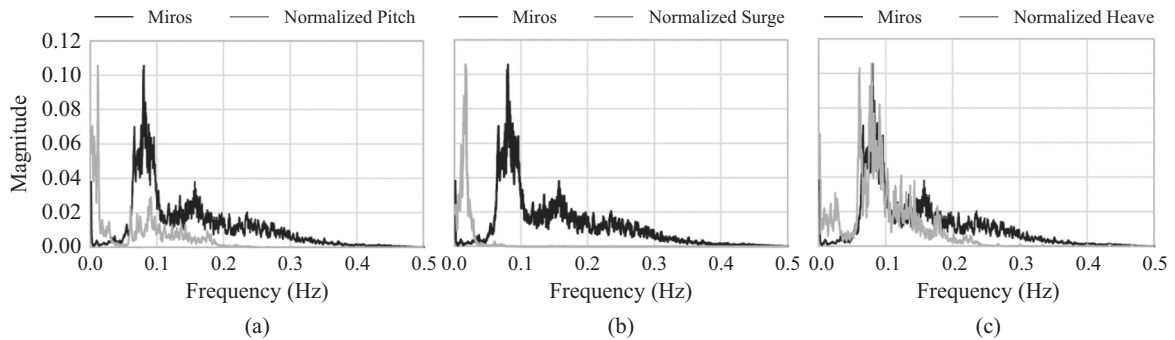

(a) (b) (c)

Fig. 17. Comparison between wave height spectrum (Miros) and Pitch spectrum (a), surge spectrum (b) and heave spectrum (c) measured with the proposed technique.

To measure the motion of the ship, as well as to calibrate the system, 6 control points were established in the Urania Mella (Fig. 12). The analysis of the displacement of the control points allowed calculating surge, heaving and pitching movements. The pictures were taken at established intervals along the day. A resolution of 4290 × 2800 px (12 Mpx) was used and the frequency of acquisition was 1 s.

The obtained results are shown in Fig. 13 and Fig. 14, where surge and heave are represented in meters measured in bow and stern regions of the ship.

Fig. 13 shows that surge measurements were almost identical in the bow and stern of the vessel, achieving both variables a correlation of 97.2%, an indication of very low measurements errors. These small differences are probably induced by the cameras reference frame distortion as a consequence of the yaw motion.

Conversely, the correlation of the two heave series was low (Fig. 14). The reason of these differences was weight and cargo variations and the time differences between waves reaching different points of the hull surface. This phenomenon produced a characteristic oscillation of the vessel, the pitch motion. Taking this into account, pitch was calculated from the differences in heave using trigonometry. The obtained values for pitch are shown in Fig. 15.

Finally, the obtained results were compared in the frequency domain with the wave heights measured near the Urania Mella with Miros radar located at the South part of the quay (Fig. 9). This high frequency vertical microwave radar provided sea level, tide and non-directional wave monitoring, with subcentimetric accuracy (+/− 5mm). Fig. 16 shows the evolution of wave height during the monitoring time and its associated spectrum. The frequency analysis revealed two predominant peaks, the most
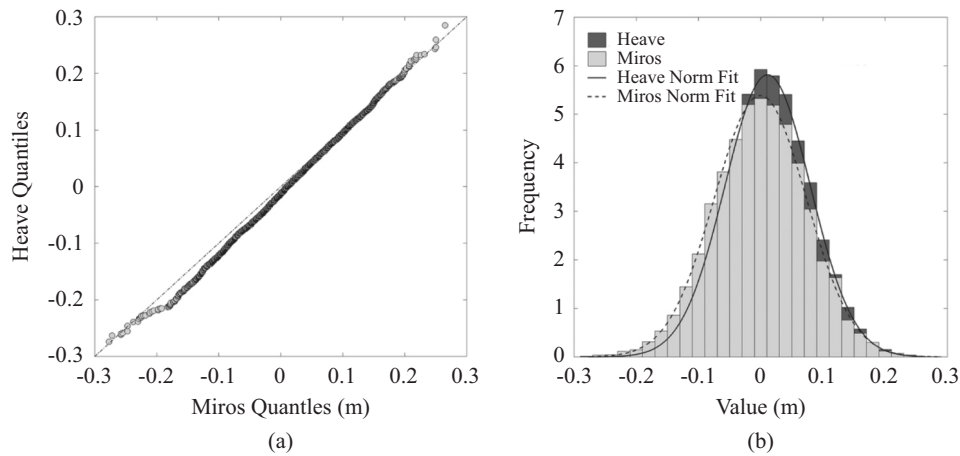
Fig. 18. QQplot (a) and Histogram-Normal PDF (b) of the heave and Miros series.

energetic (0.08 Hz) which corresponds to the peak wave period of 12.5 s, and an additional peak (0.157 Hz) associated to a period de 6.37 s, probably induced by the reflection effect of the first.

Observing Fig 17, it can be seen that the pitch movements of the ship had a frequency distribution similar to the obtained from wave elevations, with two clear peaks corresponding to oscillations of low frequency (period of 91.0 s) and high frequency (period of 11.1 s) which was close to the peak wave period. Surge, however, presented a frequency behavior not related with waves, presenting a single low frequency peak corresponding to an oscillation period of 59.7 s, and suggesting a complex oscillation behavior, probably induced by the mooring system, especially the bow and stern mooring springs which limit surge motion.

Regarding heave, the frequency distribution of this motion presented the highest similarity with the wave spectrum. Both series showed the same peak period (12.5 s). This result suggests that heave motion was closely related to wave height near the vessel. The correspondence between heave and Miros series was also analyzed comparing their quantiles. Results showed that both series came from the same type of distribution (Fig. 18(a)). Additionally, their normal probability distributions (PDF) were obtained and compared. As can be seen in Fig. 18(b), both PDFs are very similar, as occur in the frequency domain.

The obtained results validate the methodology applied to a complex real case, involving wave measurements in an outer port and ship movements. Further analysis is needed to improve the correlations between ship motions and their forcing agents.

IV. CONCLUSIONS

An optical system to study the displacements of a moored ship was designed. This system was based on the use of computer vision techniques to track feature points of the ship, allowing the measurement of the different oscillation modes of the vessel, without using expensive assemblies or on board devices.

The proposed technique was validated in laboratory conditions, comparing observed angular motions with the measurements provided by an IMU device. The results matched very satisfactorily with both techniques, showing the suitability and accuracy of the proposed approach.

Experiments in real field were conducted with the Urania Mella, an antipollution vessel moored in the Outer Port of A Coruña, in Punta Langosteira (Spain). During these assays, surge, heave and pitch were measured obtaining very promising results. In particular, heave motion recorded with the optical method showed a very satisfactory correspondence with the wave height measured by Miros Radar, both in frequency domain and in the magnitude of the registered values.

It is expected that this system may contribute to characterize the behavior of the moored ships inside the port, in order to establish limiting operation conditions, quantify the availability of the terminals, evaluate the meteorological forecast tools developed for the operation of the port, and finally establish a methodology to analyze the impact on operations of new port final layout and how to manage new traffics. Also, this system could be used as a real-time alert tool for the ship mooring security, through the simultaneous image transmission and processing.

In addition, the proposed technique can lead to stablish a more effective way of evaluating berthing and mooring equipment of the terminals, analyzing new mooring systems to reduce the downtime of the terminals and to establish recommended mooring arrangements.

REERENCES

Alderton, P. (2008). Port Management and Operations (Informa, London, United Kingdom).

Ayub, S., A. Bahraminisaab and B. Honary (2012). A Sensor Fusion Method for Smart phone Orientation Estimation. In Proceedings of the 13th Annual Postgraduate Symposium on the Convergence of Telecommunications, Networking and Broadcasting, Liverpool, England.

Bay, H., Ess, A., T. Tuytelaars and L. Van Gool (2008). Speeded-Up Robust Features (SURF). Comput. Vis. Image Underst. 110, 346-359.

Beck, R. F. and S. Liapis (1987). Transient motion of floating bodies at zero forward speed. J. Sh. Res. 31, 164-176.

Bolles, R. C., H. H. Baker and M. Hannah (1993). The JISCT stereo evaluation. In Proceedings of the Image Understanding Workshop, Washington DC, Maryland, 263.

Bont, J. De, W. Van Der Molen, J. Van Der Lem, H. Ligteringen, D. Mühlestein and M. Howie (2010). Calculations of the Motions of a Ship Moored With Moormaster TM Units. In Proceedings of the 32nd PIANC International Navigation Congress, Liverpool, United Kingdom, 622-635.

Castaldo, F. and F. A. N. Palmieri (2014). Data fusion using a Factor Graph for ship tracking in harbour scenarios. In 23rd Workshop of the Italian Neural Networks Society, Salerno, ItalyCummins, W. E. (1962). The impulse response function and ship motions. In Symposium on Ship Theory, Hamburg, Germany.

Finkelstein, A. B. (1957). The initial value problem for transient water waves. Commun. Pure Appl. Math. 10, 511-522.

Ge, S. S., C. Y. Sang and B. Voon Ee How (2011). Dynamic Positioning System for Marine Vessels. In The Impact of Control Technology, T. Samad, and A.M. Annaswamy, eds. (IEEE Contr), 137*138.

González-Marco, D., J. P. Sierra, O. Fernández de Ybarra and A. Sánchez-Arcilla (2008). Implications of long waves in harbor management: The Gijón port case study. Ocean Coast. Manag. 51, 180-201.

Grifoll, M., A. Fontán, L. Ferrer, J. Mader, M. González and M. Espino (2009). 3D hydrodynamic characterisation of a meso-tidal harbour: The case of Bilbao (northern Spain). Coast. Eng. 56, 907-918.

Hannah, M. J. (1974). Computer Matching of Areas in Stereo Images. PhD. Thesis, Stanford University.

Herbers, T. H. C., S. Elgar and R. T. Guza (1995). Generation and propagation of infragravity waves. J. Geophys. Res. 100, 24863.

Hu, J.-H., S.-S. Xu, H.-L. Chen and Z. Zhang (2009). Detection of ships in harbor in remote sensing image based on local self-similarity. J. Image Graph. 14, 591-597.

Malheiros, P., P. R. Santos, A. P. Moreira, P. Costa, F. V. Gomes and F. T. Pinto (2009). Robust and real-time motion capture of rigid bodies based on stereoscopic vision. In 3rd International Conference on Integrity, Reliability and Failure, Porto, Portugal.

Malheiros, P., P. Rosa-Santos, J. Gonçalves, P. Costa, A. Paulo Moreira, F. Veloso-Gomes and F. Taveira-Pinto (2013). Real-time tracking system for a moored oil tanker: A Kalman filter approach. In Advances in Sustainable and Competitive Manufacturing Systems, A. Azevedo, ed. (Springer Heidelberg), 749-760.

Phuong, N. H. Q., H. J. Kang, Y. S. Suh and Y. S. Ro (2009). A DCM Based Orientation Estimation Algorithm with an Inertial Measurement Unit and a Magnetic Compass. J. Univers. Comput. Sci. 15, 859-876.

Pina, G. G. and R. I.Alonso (1993). Análisis crítico de los sistemas de atraque de buques (Centro de Estudios y Experimentación de Obras Públicas (CEDEX), Gabinete de Formación y Documentación).

Rabinovich, A. B. (2009). Seiches and Harbour Oscillations. In Handbook of Coastal and Ocean Engineering, C. K. Young, ed. (World Scientific Publishing Co., Singapore), 193-236.

Rodriguez, A., J. R. Rabuñal, J. L. Perez and F. Martinez-Abella (2012). Optical Analysis of Strength Tests Based on Block-Matching Techniques. Comput. Civ. Infrastruct. Eng. 27, 573-593.

Sammartino, S., J. C. S. Garrido, J. Delgado, C. Naranjo, F. C. Aldeanueva and J. G. Lafuente (2014). Experimental and numerical characterization of harbor oscillations in the port of Málaga, Spain. Ocean Eng. 88, 110-119.

Tuytelaars, T. and K. Mikolajczyk (2008). Local Invariant Feature Detectors: A Survey. Found. Trends Comput. Graph. Vis. 3, 177-280.

Uzaki, K. ichi, N. Matsunaga, Y. Nishii and Y. Ikehata (2010). Cause and countermeasure of long-period oscillations of moored ships and the quantification of surge and heave amplitudes. Ocean Eng. 37, 155-163.

Wehausen, J. V. (1967). Initial-value problem for the motion in an undulating sea of a body with fixed equilibrium position. J. Eng. Math. 1, 1-17.

Weng, J., P. Coher and M. Herniou (1992). Camera Calibration with Distortion Models and Accuracy Evaluation. IEEE Trans. Pattern Anal. Mach. Intell. 14, 965-980.

Woodman, O. J. (2007). Introduction to Inertial Navigation (Computer Laboratory, University of Cambridge).

Zhang, Z. (1999). Flexible camera calibration by viewing a plane from unknown orientations. In Proceedings of the IEEE International Conference on Computer Vision, Kerkyra, Greece.